Journal Pre-proofs

Research paper

Synthesis, Characterisation and Crystal Structure of a new Cu(II)-Carboxamide Complex and CuO Nanoparticles as new Catalysts in the CuAAC Reaction and Investigation of their Antibacterial Activity

Mahsa Kiani, Mojtaba Bagherzadeh, Soraya Meghdadi, Farzaneh Fadaei-Tirani, Maryam Babaie, Kurt Schenk-Joß

PII: S0020-1693(19)31843-2
DOI: https://doi.org/10.1016/j.ica.2020.119514
Reference: ICA 119514

To appear in: *Inorganica Chimica Acta*

Received Date: 27 November 2019
Revised Date: 8 February 2020
Accepted Date: 9 February 2020

Please cite this article as: M. Kiani, M. Bagherzadeh, S. Meghdadi, F. Fadaei-Tirani, M. Babaie, K. Schenk-Joß, Synthesis, Characterisation and Crystal Structure of a new Cu(II)-Carboxamide Complex and CuO Nanoparticles as new Catalysts in the CuAAC Reaction and Investigation of their Antibacterial Activity, *Inorganica Chimica Acta* (2020), doi: https://doi.org/10.1016/j.ica.2020.119514

Synthesis, Characterisation and Crystal Structure of a new Cu(II)-Carboxamide Complex and CuO Nanoparticles as new Catalysts in the CuAAC Reaction and Investigation of their Antibacterial Activity

Mahsa Kiani [a], Mojtaba Bagherzadeh [a]*, Soraya Meghdadi [b], Farzaneh Fadaei-Tirani [c], Maryam Babaie [b] and Kurt Schenk-Joß [d]

[a]*Department of Chemistry, Sharif University of Technology, Tehran 11155-3516, Iran*

[b]*Department of Chemistry, Isfahan University of Technology, Isfahan 84156-83111, Iran*

[c]*Institute of Chemical Sciences and Engineering, École Polytechnique Fédérale de Lausanne, CH-1015 Lausanne, Switzerland.*

[d]*Institute of Physics, École Polytechnique Fédérale de Lausanne, CH-1015 Lausanne, Switzerland.*

Corresponding authors: M. Bagherzadeh,

**E-mail address*: bagherzadeh@sharif.edu

Abstract

The bidentate carboxamide ligand N-(thiazole-2-yl) picolinamide (**LH**) was synthesized in the environmentally friendly ionic liquid TBAB, and the five-coordinated Cu^{II}-complex, $[Cu(L)_2(H_2O)].CHCl_3$ (**1**) was synthesized from **LH** and copper(II)acetate. Cupric oxide [CuO] nanoparticles (**2**) have been prepared by the thermal decomposition of (**1**) as a new precursor at 600°C for 3 h under air atmosphere. (**1**) was characterised using FT-IR spectroscopy, elemental analyses and its solid state structure was confirmed by single crystal X-ray diffraction. (**2**) were identified by FT-IR spectroscopy, X-ray powder diffraction, scanning electron microscopy, energy dispersive X-ray analysis and thermo-gravimetric differential thermal analyses. The electrochemical behaviour of **LH** and (**1**) has been investigated by cyclic voltammetry: irreversible $Cu^{II/I}$ reductions were observed. The catalytic activity of (**1**) and (**2**) were evaluated in the one-pot azide–alkyne cycloaddition click reaction in water without additional agents. **LH**, (**1**) and (**2**) were also screened for their *in vitro* antibacterial activity: they showed promising antibacterial activity comparable to that of the antibiotic penicillin.

Keywords**:** N-(thiazole-2-yl) picolinamide; Cu(II)-carboxamide complex; Copper oxide; Azide–alkyne cycloaddition and antibacterial activity.

Introduction

The concept of "click chemistry" has revolutionised molecular engineering including applications to organic and medicinal chemistry [1, 2] and polymer and material science [3]. Numerous analyses have shown Cu^{2+} to be able to catalyse several mechanisms such as cycloaddition reactions between azides and alkynes (a typical click reaction) as well as other types of click reactions [4-7]. Applying Cu^{2+} nanoparticles [NP] to catalyse the specific click reaction associated with a carboxamide-based ligand would appear to be a promising approach for designing and implementing a highly efficient catalyst [8-10].

Cost-awareness is primordial in designing an experiment and scaling it up to the industrial phase, but high purity and suitable isomerisation of the desired compound without losing sight of an easy conversion to technology [11] are hardly less important. If the catalyst could be green, efficient and affordable, we would have achieved something truly promising [12].

In the industrial and laboratory phases, catalytic reactions functionalising C-H bonds are being considered important owing to their economic and ecologically benign nature. The scale-up of this series of reactions requires that they be sustainable, cost-effective and one-pot reactions. There seems to be a consensus that a one-pot reaction requires the use of expensive transition metals such as ruthenium and palladium [13-18]. Logically, sustained efforts are currently devoted to finding a greener catalyst working with cheaper metals. Numerous attempts at finding green and highly reproducible ways of synthesising organic and inorganic compounds have been undertaken in the last decade[19]. Ideally, these ought to be inexpensive, too. At present, one of the largest barriers to the industrialization of organic and inorganic compounds is the use of organic solvents. Perhaps the most important tenet of green chemistry is the use of harmless green solvents capable of increasing the reaction rate and the efficiency. For a catalytic

application it is primordial to design a high-performance system and relentlessly apply the optimised strategy [20-22].

In an intense search for suitable alternatives to hazardous solvents, ionic liquids (ILs) have emerged as the top-choice for a sustainable chemistry[23, 24]. But even ILs come with their own risks and perils, such as toxicity and flammability. In our study, we used molten tetrabutyl-ammonium bromide [TBAB] which was shown to be safe and clean in numerous studies; it can be considered a suitable catalyst for this type of reactions [25-29].

Carboxamide-based compounds play a role in several fields owing to their potential applications in biomedical science[30, 31], catalytic processes[32, 33] and sensors[34-36]. The heart of these compounds is the carboxamide linkage, –C(O)NH–, considered as one of the most vital and essential functional groups in nature, and also an important concept in bio-inspired studies[37, 38]. The conventional method for the synthesis of carboxamide-based compounds consists in the typical reaction between an appropriate carboxylic acid and the corresponding amines in an organic solvent, for instance pyridine, and, possibly, in the presence of an activator. This conventional method is not much fancied by green chemistry because of its low yield and the toxicity of the organic solvent[39]. Several critical applications have, however, traditionally been optimised in the conventional procedure. Nowadays, extensive investigations have been devoted to engineering non-toxic carboxamides for catalytic and biomedical applications [40-43]. Catalytic application of this kind of ligand is judged a promising way of improving the bench-scale and scale-up phases of some crucial mechanisms. The design and synthesis of organometallic complexes from these ligands then becomes a primordial task [44, 45].

Advances in nm-sized metal and metal oxide particles in several shapes have sparked important and vital developments in both science and technology. Preparation of these NPs lies in the

hands of chemists, who are able to skilfully design an experiment, optimise it and implement several procedures for obtaining the NPs, but their application mostly profits process and biomedical engineering and, in some cases, the catalysis of the fundamental chemical reactions in chemistry [46-49].

Cupric oxide [CuO] (Tenorite) is a p-type metal-oxide semiconductor widely applied in gas sensors, electrochemical and solar cells, photoconductive and thermoelectric materials owing to its unique catalytic and electrical properties. Recently, it has also been used as an antimicrobial agent against various bacterial species [50].

We have synthesised the bidentate carboxamide ligand N-(thiazole-2-yl) picolinamide [**LH**] in TBAB serving as the reaction medium and catalyst. The complex (**1**) was prepared using **LH** and copper(II) acetate; then (**1**) was thermally decomposed to give CuO NPs (**2**). (**1**) was characterised using FT-IR, elemental analysis, CV and X-ray diffraction. (**2**) was identified by FT-IR, XRD, FESEM, EDX and TGA-DTA. The catalytic properties of (**1**) and (**2**) were assessed in the one-pot azide-alkyne cycloaddition [AAC] reaction in the presence of water as a solvent without any additional reducing agents or bases. (**1**) and (**2**) were furthermore investigated regarding their antibacterial activity.

2. Experimental

2.1. Materials and General Methods

All solvents and chemicals were of commercial reagent grade and used as received from Aldrich and Merck. Elemental analyses were performed by using a Carlo ERBA Model EA 1108 elemental analyser. UV–Vis spectra were recorded on a JASCO V-570 spectrophotometer. Infrared spectra (KBr pellets) were obtained using a Unicam Matson 1000 FT-IR spectrophotometer. The ^{1}H NMR spectra of the ligand was obtained on a Bruker FT-NMR 500

MHZ spectrometer; proton chemical shifts are reported in parts per million [ppm] relative to an internal standard of Me_4Si. Cyclic voltammograms were recorded by using a SAMA 500 Research Analyser. Three electrodes were utilized in this system, a glassy carbon working electrode, a platinum disk auxiliary electrode and a silver wire as the reference electrode. The glassy-carbon working-electrode (Metrohm 6.1204.110) of a 2.0 ± 0.1 mm diameter was manually cleaned with 1-mm alumina and polished prior to each scan. Tetra butyl ammonium hexafluorophosphate (TBAH) was used as the supporting electrolyte. The solutions were deoxygenated by purging with Ar for 5 min. All electrochemical potentials were calibrated versus the internal Fc+/o (E8 = 0.40 V vs. SCE) couple under the same conditions. Thermogravimetric-differential thermal analysis (TG-DTA) was conducted on a Netzsch STA 449F3 thermal analyser at a constant heating rate of 10°C min^{-1} in air. An X-ray (λ=1.54060Å) powder diagram was recorded in $25 \leq 2\theta \leq 100°$ at 25ºC with a step-size of 0.05° on an MPD PRO from PANalytical. The morphology and composition of CuO NPs were observed by field emission scanning electron microscopy (FESEM, MIRA3 TESCAN) and FE-SEM coupled energy-dispersive X-ray spectroscopy (EDX).

2.2. Synthesis of N-(thiazole-2-yl) Picolinamide (LH)

A mixture of 3.22 g (10 mmol) of triphenylphosphite, 1.61 g (5 mmol) of TBAB, 1.23 g (10 mmol) of picolinic acid and 1 g (10 mmol) of 2-aminothiazole in a 25 mL round-bottomed flask was placed in an oil bath. This reaction mixture was heated until it formed a homogeneous solution which was then stirred for 1 h at 120˚C. The viscous solution was then cooled to room temperature and treated with 5 mL cold methanol. The resulting light yellow solid was filtered-off and washed with cold methanol. Yield 79%. Anal. Calc. for $C_9H_7N_3OS$ (205.32 g mol^{-1}): C, 52.67; H, 3.44; N, 20.47; S, 15.61. Found: C, 52.31; H, 3.46; N, 20.34; S, 15.21% .FT-IR (KBr,

cm^{-1}) ν_{max}: 3175 (NH), 1675 (C=O_{amide}), 1525 (C-N) cm^{-1}. UV–visible (Acetonitrile) λ_{max} (nm) (ε, L mol^{-1} cm^{-1}): 287 (32,800), 221 (32,440). ^{1}H NMR (CDCl3, 500 MHz): 7.36 (d, H_c), 7.58 (d, H_b), 7.73 (m, H_e), 8.12 (m, H_f), 8.19 (d, H_d), 8.77 (d, H_g), 11.94 (s, NH).

2.3. Synthesis of [Cu(L)$_2$(H$_2$O)].CH$_3$Cl (1)

For the synthesis of this complex, 0.041 g (0.199 mmol) of the ligand **LH** were dissolved in 20 mL of chloroform and then 0.02 g (0.1 mmol) of copper(II) acetate were added to this solution. This reaction solution was stirred for 2 h and then filtered. Then 20 mL of ethanol were added to the filtrate and the green solution left to evaporate in a refrigerator. After some time green crystals of (**1**) suitable for X-ray diffraction had grown and were isolated by filtration, washed with cold ethanol and dried in vacuum. Yield 76%. Anal. Calc. for $C_{19}H_{15}Cl_3CuN_6O_3S_2$: C, 37.45; H, 2.48; N, 13.79; S, 10.59. Found: C, 38.2; H, 2.408; N, 14.03; S, 10.92%. FT–IR (KBr, cm^{-1}) ν_{max} = 1627 (C=O_{amide}), 1583 (C-N) cm^{-1}. UV–visible (Acetonitrile) λ_{max} (nm) (ε, L mol^{-1} cm^{-1}): 709 (240), 324 (26,400), 280 (35,200), 261 (47,200).

2.3. Preparation of Nanoparticles of Cupric Oxide (2)

CuO NPs of (**2**) were prepared by the thermal decomposition of (**1**). A very small amount of (**1**) was loaded into a crucible and then placed in oven and heated at a rate of 10°C/min in air. NPs of CuO were obtained after heating at 600°C for 3 hours. The resulting NPs were characterized by FT-IR, FE-SEM and XRD analysis.

2.4. Biological Studies

The ligand **LH**, the Cu(II) complex (**1**) and the CuO NPs (**2**) were individually tested against a panel (Gram negative and Gram positive) of microorganisms, namely *Bacillus cereus* and *Staphylococcus aureus* as Gram +ve and *Salmonella typhi, Klebsiellap neumoniae* and

Escherichia coli as Gram –ve species. The organisms were grown by the well-known diffusion method using Sabouraud-dextrose and Müller-Hinton agar. The minimum zone of inhibition [MZI] was recorded upon the completion of the incubation and the mean diameter for each complex at 300 μg mL^{-1} was recorded. Stock solutions of the compounds were prepared in dimethylsulfoxide. The MZI produced by the compounds were compared with those of the standard antibiotic penicillin at similar concentrations. Each test was carried out three times to minimize the error. In order to clarify any effect of DMSO in the biological screening, blank studies were carried out, and no activity was observed against any bacterial strains in pure DMSO.

2.5. General Procedure for the CuAAC Reaction

To a reactor containing alkyne (0.5 mmol), the organic halide (0.55 mmol), NaN_3 (0.55 mmol) and H_2O (2 mL), either (**1**) or (**2**) were added as the catalyst. The reaction mixture was stirred at 70 °C for 4-6 h and the completion of the reaction was judged by thin layer chromatography. Water (5 mL) was then added to the resulting mixture and the product was extracted with ethyl acetate (2 x 10 mL) from the aqueous phase. The organic layer was dried over anhydrous $MgSO_4$ and the solvent was removed under reduced pressure to give the corresponding 1,2,3-triazoles. Further purification was necessary in the case of complex **1,** since it was not soluble enough in ethyl acetate. To obtain the pure products, after extraction with ethylacetate, the reaction mixture was filtered and the residue was subjected to column chromatography (eluent, 40% EtOAc in n-hexane).

2.6. X-ray Crystallography

Green crystals of **1** suitable for X-ray diffraction were obtained from ethanol and dichloromethane. Bragg intensities of **1** were collected, at room temperature, on a Stoe IPDS II

using graphite-monochromatized Mo *K*α (λ = 0.71073 Å) with the help of X-Area WinXpose [51]. The cell refinement was carried out by means of X-Area Recipe [52], data reduction and a numerical absorption correction, based on the habitus, with X-Red32 [53] and X-Area Integrate [54].

The solution and refinement of the structure were performed by the latest available versions of ShelXT[55] and ShelXL[56]. All non-hydrogen atoms were refined anisotropically using full-matrix least-squares based on $|F|^2$. The hydrogen atoms were placed at calculated positions by means of the "riding" model in which each H-atom was assigned a fixed isotropic displacement parameter with a value equal to 1.2 U_{eq} of its parent C-atom (1.5 U_{eq} for the methyl groups), but hydrogen atoms of coordinated water molecule were found in a difference map and refined freely. Details of the data collection, structure solution and refinement of **1** are compiled in Table 1.

In the structure **1**, the solvent molecule of chloroform is disordered over two positions which could be located in a difference map and refined anisotropically, yielding site occupancy ratios of 0.56(6)/0.44(6), but SADI restraints were used to optimise the bond lengths and SIMU restraints were applied to refine the displacement-ellipsoids of the atoms.

3. Results and discussion

3.1. Synthesis of the Ligand and the Complex

The ligand **LH** was synthesised in the IL TBAB in order to decrease the reaction time, increase the efficiency and reduce the risks of toxic solvents such as pyridine. The complex (**1**) was synthesised by the reaction of **LH** with copper(II) acetate. Green crystals of (**1**) suitable for X-ray diffraction were obtained by slow evaporation from ethanol and dichloromethane at refrigerator temperature.

3.2. Description of the Structure of (1)

The complex (**1**) is shown in Fig. 1 and some of its geometrical details are given in Table 2. The complex crystallizes in the monoclinic space group $P2_1/n$ with four complexes in the unit cell. The ligand **LH** is bidentate and coordinates to the Cu^{2+} ion via its carboxamide nitrogen and its nitrogen of the pyridine ring. The oxygen atom of a water molecule completes the coordination-pyramid; its ADDISON parameter of 0.26 for (**1**) confirms the Jahn-Teller "axially" elongated square pyramidal coordination (the N6 pyridine atom occupying the long axial position of the Cu(II) ion). The lengths of the bonds for $Cu\text{-}N_{amid}$ [$Cu\text{-}N_2$= 2.006(2), $Cu\text{-}N_5$= 1.990(2)] and $Cu\text{-}N_{pyridyl}$ [$Cu\text{-}N_3$= 2.027(3), $Cu\text{-}N_6$= 2.227(3)] are comparable to the lengths of those bonds observed in analogous copper complexes [18-20]. The length of the $Cu\text{-}N_{amid}$ bonds is slightly shorter than that of $Cu\text{-}N_{pyridyl}$. The trans angles around the central ion [$N_5\text{-}Cu\text{-}N_6$= 77.67(10)°, $N_2\text{-}Cu\text{-}N_6$= 106.98(10)°, $N_3\text{-}Cu\text{-}N_6$= 99.68(11)°, $N_6\text{-}Cu\text{-}O_3$= 101.62(11)°] deviate from the value 90° for the ideal square pyramid structure. It is also observed that the two equatorial angles [$N_2\text{-}Cu\text{-}N_3$=81.45(11)°] and [$N_5\text{-}Cu\text{-}O_3$=89.17(10)°] are smaller than 90° and two equatorial angles [$O_3\text{-}Cu\text{-}N_2$= 93.18(10)°] and [$N_5\text{-}Cu\text{-}N_3$= 94.47(11)°] are greater than 90°. This indicates a pressure in coordination space owing to the strong ligand structure. Information about important hydrogen bonds in (**1**) is given in the Table 3; there is an intramolecular O3-H3B⋯⋯N1 hydrogen bond involving the coordinated water O3 and the N1 nitrogen of the thiazole, an intermolecular O3-H3A⋯⋯O2 one again between the water O3 and the carboxamide oxygen O2 and, finally, quite a few weak C-H⋯⋯O and C-H⋯⋯Cl hydrogen bonds.

3.3. Spectroscopic properties

The FT-IR spectral data of **LH**, (**1**) and the nanoparticle (**2**) are shown in Fig S1 and Fig 2, respectively. The FT–IR spectra of the free ligand exhibit a band at 3178 cm^{-1}, which corresponds to $\nu(NH_{amidic})$; the absence of this stretching band in the spectra of the corresponding Cu(II) complex confirms that the ligand is coordinated in its deprotonated form [57]. The decrease of the carbonyl stretching frequency of the ligand upon complex-formation furnishes a further indication of the coordination of the deprotonated amide. The sharp C=O stretching vibration bands at 1676 cm^{-1} are red-shifted to 1627 cm^{-1} for (**1**), which is in accordance with the data reported for the related complexes [58].

The observation of a significant increase in the frequency of C–N stretching vibration of medium intensity for the coordinated $\mathbf{L}^{1-}$ (1583 cm^{-1}) relative to the free ligand (1525 cm^{-1}) gives additional support to the coordination of the amide in the deprotonated form. This blue-shift is presumably due to the resonance enhancement in the deprotonated amide which in turn leads to the strengthening of C–N bond[59, 60].

In the FT-IR spectra of the calcination products, presented in Fig. 2b, no relevant peaks indicating the presence of organic ligands or fragments are observed. However, the appearance of two strong bands (at 535 and 580 cm^{-1}) in the FT-IR spectra of the thermal decomposition products confirms the tenorite structure of CuO as the decomposition product [61]. The broad band at about 3434 cm^{-1} and a weak band at 1628 cm^{-1} are assigned to adsorbed water.

The electronic absorption spectrum of **LH** in acetonitrile is shown in Fig S2. This spectrum includes two bands at 221 and 287 nm, assigned to the intra-ligand transitions ($\pi \rightarrow \pi^*$ of aromatic rings and $n \rightarrow \pi^*$). The UV-Vis spectrum of the $[Cu(L)_2(H_2O)].CH_3Cl$ complex is shown in Fig. 3.

This complex has a distorted square pyramid structure. The copper centre has a d^9 configuration, so it presents d-d transitions. The green colour of the complex is due to the presence of an absorbent band in the 500-800 nm region. The absorption bands at 324, 280 and 261 nm, observed in the electron spectrum, are related to the displacements of charge and intra-ligand transitions. Also, the absorption band at 703 nm is related to a d-d transition.

Fig. 4 shows the thermogram of the $[Cu(L)_2(H_2O)].CH_3Cl$ precursor indicating that the decomposition of the complex (**1**) takes place in two steps. A significant mass change (Found 21.91%, Calc. 21%) starting at 128 °C corresponds to the expulsion of water and CH_3Cl molecules. An exothermic process (sharp exothermic peak at 670°C) with a weight loss of 69.37% is related to the decomposition of the ligand and the production of cupric oxide CuO. The structure of CuO (tenorite) is confirmed by FT-IR and XRD.

The X-ray powder diagram of CuO, obtained from the thermal decomposition of (**1**) at 600 °C for 3 h, is shown in Fig. 5. The diagram can be indexed in the monoclinic cell 4.6797(5), 3.4314(4), 5.1362(6); 99.262(5) and the space group C2/c (04-015-5876)[62, 63].

These results confirm that the (**1**) is completely decomposed into the cupric oxide phase at 600 °C, in good agreement with the TG-DTA and FT-IR results. The crystallite size of the as synthesized product, D_c, was calculated from the average of the major diffraction peaks using Scherrer's equation (Eq(1)) [64]:

$$D_c = K\lambda / \beta cos\theta \,, \qquad (1)$$

where K is a constant (ca. 0.9); λ is the X-ray wavelength used in *XRD* (1.5418 Å); θ the Bragg angle; β is the pure diffraction broadening of a peak at half-height, i.e., the broadening due to the dimensions of the crystallites. The size of the NPs calculated according to Scherrer's equation from Fig. 5, is 39 nm.

The size and morphology of the cupric oxide NPs were investigated by scanning electron microscopy (FESEM) .The FESEM images and size distribution of the CuO NPs are shown in Fig. 6. as can be seen, cupric oxide NPs are sphere-like and the average particle size is 39 nm. The particles have a uniform size, a homogeneous sphere-like morphology and a narrow size distribution. The image clearly shows the aggregation of grains of high surface area.

The chemical composition of the prepared CuO was investigated by using energy dispersive X-ray analysis (EDX). As observed in Fig. 7, EDX analysis of the CuO NPs confirms the presence of copper and oxygen in structure. Comparison of copper and oxygen peak intensities are compatible with the XRD findings, namely that these particles mainly consist of cupric oxide. The peak characteristic of carbon is probably due to the coating of the grid [65].

3.4. Electrochemical Studies

The electrochemical behaviour of **LH** and (**1**) have been studied by cyclic voltammetry in DMF solution at a scan rate of 100 mVs^{-1}, with 0.1 M TBAH as the supporting electrolyte at a glassy carbon working electrode. As expected and previously reported, the carboxamide ligands are electro-active in common organic solvents[66]. As shown in the voltammogram of **LH** (Fig. 8), the two irreversible reduction waves of thiazole and pyridine rings are observed at -2.3 V and -1.54 V and are shifted for the Cu(II) complex (**1**).

The electrochemistry of $[Cu(L)_2(H_2O)_2].CHCl_3$ in DMF (Fig. 9) shows an irreversible $Cu^{II/I}$ reduction peak at -0.45 V and an irreversible $Cu^{I/II}$ peak at 0.36 V. Also, in this voltammogram, an irreversible reduction peak of a solvation complex, due to the partial solvation of the central metal, is observed at a potential of 0.01 V and the oxidation peak at a potential of 0.06 V. The irreversible reductions observed at the potentials -2.01 and -2.38 V are related to pyridine and thiazole rings, respectively.

3.5. Catalytic Activity

The catalytic activity of complex (**1**) and CuO (**2**) for the AAC reaction were investigated. Following previously published work [67], we initially considered the reaction between phenyl acetylene and benzyl chloride with sodium azide as the model reaction for complex (**1**). To obtain the optimal reaction conditions, the critical parameters such as catalyst loading, solvent, base, temperature and time of reaction were compared (Table 4). In our first set of experiments, a blank reaction with no catalyst was studied (Table 4, entry 1); as expected no conversion to the product was observed. In subsequent experiments, an aqueous solution of phenyl acetylene (0.5 mmol) and benzyl chloride (0.55 mmol) was allowed to react with sodium azide (0.55 mmol) in the presence of different loadings of catalyst from 0.54 mol% to 2.59 mol%. Heating the reaction mixture to 70 °C afforded the AAC reaction product with 79% (entry 2) to 99% (entry 6) after 6 h. A further increase in the amount of catalyst to 5.18 mol% afforded no improvement in the yield (Table 4, entry 7).

The analogous procedure showed the optimal amount of catalyst (**2**) to be 1.35 mol% with a 95% yield (entry 12); unsurprisingly, the results depended on the amount of catalyst (entry 13) used. It was also found that temperature has an essential effect on this catalytic system. As can be seen in Table 4, for catalyst (**1**), at room temperature, the yield obtained was only 11% (entry 14). By increasing the temperature from 40 to 60 °C, the product yield increased to 66% and 84% (entries 15-17). The most suitable temperature for the AAC reaction in the presence of catalyst (**1**) was 70 ˚C (Table 4, entry 6). The analogous values for the catalyst (**2**) were 70 °C and a yield of 95% (entry 12). The reaction was considered completed after 6 h, but an effective improvement in the yield of the triazole was observed when decreasing the reaction time from 6 to 4 h (entries 22 and 23, Table 4), but the yield of the reaction decreased. To establish the

optimal conditions for the catalyst, the effect of various solvents on the model reaction was investigated in-depth (Fig. 10). The results of these experiments reveal that among the different solvents screened such as (methanol, dichloromethane, water, ethanol, acetone, toluene, and chloroform), water can be used as a green, inexpensive and efficient solvent for AAC reaction. Under the optimised reaction conditions (Table 3, entry 6 for catalyst (**1**) and entry 12 for catalyst (**2**)) a variety of diversely substituted phenyl acetylenes with a mixture of benzyl bromides/chlorides and sodium azide to generate the desired 1,2,3-triazoles (Table 5) were studied. Electron withdrawing and electron donating groups on the phenyl ring of the benzyl halides and the phenyl acetylenes have little effect on the yield of the reaction (entries 2-6). Furthermore, steric hindrance and coordination ability of substrates to the Cu centre were observed for *ortho* substituents on the benzyl chloride as compared to the *para* derivatives (entries 2 and 3), for instance, that *o*-methyl benzyl chloride was less reactive than *p*-methyl benzyl chloride. Steric effects also seem to cause the fact that the *ortho*-substituted groups needed longer reaction times to afford the corresponding products in an acceptable yield than those obtained with *para*-substituted ones. We also observed that aliphatic alkynes require longer reaction times to give high yields compared with aromatic alkynes, which seems to indicate that the reactivity of the substrate is low. When propargyl alcohol or 2-methyl-3-butyn-2-ol was used as a terminal alkyne, the reaction proceeded smoothly to give the corresponding products in moderate yields (entries 7, 8, 12 and 13). The lower reaction yields are probably due to the complexation of copper by alcoholic hydroxy groups[68]. Furthermore, 2-methyl-3-butyn-2-ol gave lower yields compared to the propargyl alcohol owing to the high steric hindrance. Replacing benzyl chloride with benzyl bromide for both catalysts seemed to indicate that benzyl chloride is slightly more reactive than benzyl bromide (entries 9-13).

From the vantage point of green chemistry, reusability is one of the most important properties of any metal catalysis. In this regard, the reusability of catalyst (**1**) and (**2**) were studied by monitoring successive cycles of the AAC reaction of phenyl acetylene, benzyl chloride and NaN3 under the optimised reaction conditions. After the first catalytic cycle, the catalyst was easily separated by filtration from the reaction mixture, washed with ethanol and acetone (3 × 5 mL) and dried at 55 ˚C for 1 h. Then, a new AAC reaction of fresh reactants was started using the recovered catalyst. The catalysts were seen to be stable and reusable for up to four runs during the catalytic reaction as they afforded almost identical results in each cycle, but a slight decrease in the yields was observed and the reaction yield reduced to 81% for catalyst (**1**) and 79% for catalyst (**2**) (Fig. 11). This decrease in the catalytic activity was judged to be due to the decomposition of the complexes and structural changes.

We designed two reactions for investigating the active copper species performing the catalytic reaction according to previous papers [69], with a 2:1 ratio of sodium ascorbate:catalyst (sodium ascorbate is used as a mild reducing agent) in the catalytic system and the results are presented in Table 4, (entries 24 and 25). No progress of efficiency could be detected by adding a reducing agent.

The reduction of Cu(II) to Cu(I) during the catalytic reaction was extensively studied by means of EPR and UV analysis [70]; it was found that the active species for the catalytic reaction is copper(I). If copper(II) is used as catalyst for the AAC reaction, it must therefore be reduced to copper(I) and only then the catalytic reaction cycle can start. In the absence of a reducing agent, the real catalytic Cu(I) species was generated within a short induction period via reducing Cu(II) salts by alcohol oxidation, homocoupling of terminal alkyne[71-74] or sodium azide [74, 75]; in

the present case, in which there were no alcoholic solvents, Cu(II) had to be reduced through homocoupling of terminal alkyne or by sodium azide.

Let us finally compare the catalytic reactivity of catalysts (**1)** and (**2**) with recently reported catalytic systems for the AAC reaction. Our catalysts work without the need of an inert atmosphere or additional reducing agents. Furthermore, the previously reported systems often require higher amounts of catalysts (entries 1-4 and 8), higher temperature (entries 4 and 8), more solvent (entries 1, 2, 4, 7 and 9) or longer reaction times (entries 2, 4-7) for the reaction to progress. Other advantages of our catalysts are: in situ generation of organic azides, simple preparation of the catalysts, easy and quick isolation of products and the use of water as a green solvent.

3.6. Antibacterial studies

The ligand **LH** and its corresponding Cu(II) complex (**1**) and CuO nanoparticles (**2**) were tested for antibacterial activity against *Bacillus cereus* and *Staphylococcus aureus* as Gram +ve and *Salmonella, Klebsiella pneumoniae* and *Escherichia coli* as Gram –ve species. The screening results (MZI) are summarized in Fig. 12. While **LH** does not show significant activity, it is evident that the compounds **1** and **2** exhibit antibacterial activity comparable to that observed for the standard antibiotic penicillin. The inertness of the metal-ligand linkage presumably increases its lipophilicity, cell permeability, and protection against enzymatic degradation [76]. However, the exact mechanism is unclear yet and further biological studies are necessary to get a clear picture of this behaviour [77].

In this study, the cupric oxide nanoparticles showed remarkable antibacterial activity against both Gram-positive (*S. aureus*) and Gram-negative (*E. coli and kelebseilla*) bacteria (Fig. 12). The observed extent of inhibition of bacterial growth suggests that the antibacterial activity of

CuO nanoparticles (**2**) is higher than that of the Cu (II) complex (**1**). This is in accord with previously reported works [63].

Conclusions

The carboxamide ligand *N-(thiazole-2-yl) picolinamide* (**LH**), has been synthesised in the ionic liquid TBAB and characterised; this benign way increased the product-yield and reduced the reaction-time. The complex $[Cu^{II}(L)_2(H_2O)].CHCl_3$ and cupric oxide NPs (tenorite) have been synthesised, characterised and assessed as catalysts in the AAC reaction for two dozens of typical compounds. Crystals of the Cu^{II}-complex were grown from ethanol/dichloromethane, studied by X-ray diffraction and their structure discussed. The electrochemical study of the Cu^{II}-complex revealed a $Cu^{II/I}$ reduction process important for the catalytic activity. The Cu^{II}-complex catalysed the AAC reaction under mild conditions and excellent yields in a short reaction time under aerobic conditions in water and the Cu(II)-complex is more reactive than CuO NPs. The ligand **LH**, the Cu^{II}-complex and the cupric oxide NPs were also screened for their *in vitro* antibacterial activity: the complex and CuO present strong biological activity comparable to that of the antibiotic penicillin, while the ligand is not active; the antibacterial activity of the cupric oxide NPs is higher than that of the Cu^{II}-complex.

Acknowledgments

Support of this work by the Research Council of Sharif University of Technology is gratefully acknowledged**.**

Appendix A. Supplementary Material

The CCDC number 1952723 contains the crystallographic data for the compound **(1),** namely **[Cu(L)$_2$(H$_2$O)].CH$_3$Cl**, in this paper. These data can be obtained, free of charge, from www.ccdc.cam.ac.uk/data_request/cif.

References

[1] C.A. DeForest, B.D. Polizzotti, K.S. Anseth, Nature materials, 8 (2009) 659.
[2] N.P. Grimster, B. Stump, J.R. Fotsing, T. Weide, T.T. Talley, J.G. Yamauchi, Á. Nemecz, C. Kim, K.-Y. Ho, K.B. Sharpless, Journal of the American Chemical Society, 134 (2012) 6732-6740.
[3] P.L. Golas, K. Matyjaszewski, Chemical Society Reviews, 39 (2010) 1338-1354.
[4] D. Li, W. Zhou, Y. Chai, R. Yuan, Y. Xiang, Chem. Commun., 51 (2015) 12637-12640.
[5] E. Doustkhah, M. Heidarizadeh, S. Rostamnia, A. Hassankhani, B. Kazemi, X. Liu, Mater. Lett., 216 (2018) 139-143.
[6] Z. Hu, J. Hu, Y. Cui, G. Wang, X. Zhang, K. Uvdal, H.-W. Gao, Journal of Materials Chemistry B, 2 (2014) 4467-4472.
[7] M.S. Singh, S. Chowdhury, S. Koley, Tetrahedron, 72 (2016) 5257-5283.
[8] R.S. Chauhan, D. Oza, S. Yadav, C. Dash, A.M. Slawin, N. Shivran, New Journal of Chemistry, 43 (2019) 2381-2388.
[9] C.-C. Chuang, H.-C. Chu, S.-B. Huang, W.-S. Chang, H.-Y. Tuan, Chemical Engineering Journal, 379 (2020) 122285.
[10] T. Tamoradi, H. Veisi, B. Karmakar, J. Gholami, Materials Science and Engineering: C, 107 (2020) 110260.
[11] S. Maiti, N. Roy, L.T. Babu, P. Moharana, C. Athira, E.D. Sreedhar, S. De, S.A. Kumar, P. Paira, New Journal of Chemistry, (2020).
[12] M. Trujillo, C. Hull-Crew, A. Outlaw, K. Stewart, L. Taylor, L. George, A. Duensing, B. Tracey, A. Schoffstall, Molecules, 24 (2019) 973.
[13] L. Ackermann, H.K. Potukuchi, D. Landsberg, R. Vicente, Org. Lett., 10 (2008) 3081-3084.
[14] L. Ackermann, A. Althammer, Angew. Chem. Int. Ed., 46 (2007) 1627-1629.
[15] C.G. Dong, Q.S. Hu, Angew. Chem. Int. Ed., 45 (2006) 2289-2292.
[16] V. Aucagne, K.D. Hänni, D.A. Leigh, P.J. Lusby, D.B. Walker, J. Am. Chem. Soc., 128 (2006) 2186-2187.
[17] P. Appukkuttan, W. Dehaen, V.V. Fokin, E. Van der Eycken, Org. Lett., 6 (2004) 4223-4225.
[18] A. Banan, F. Nikbakht, S. Ataie, Journal of Porous Materials, (2019) 1-7.
[19] S. Kwok, Nature, 430 (2004) 985.
[20] G. Rothenberg, Catalysis: concepts and green applications, John Wiley & Sons, 2017.
[21] I. Chorkendorff, J.W. Niemantsverdriet, Concepts of modern catalysis and kinetics, John Wiley & Sons, 2017.
[22] S. Ghazali-Esfahani, H. Song, E. Păunescu, F.D. Bobbink, H. Liu, Z. Fei, G. Laurenczy, M. Bagherzadeh, N. Yan, P.J. Dyson, Green Chemistry, 15 (2013) 1584-1589.
[23] R.D. Rogers, K.R. Seddon, Science, 302 (2003) 792-793.
[24] P. Wasserscheid, T. Welton, Ionic liquids in synthesis, John Wiley & Sons, 2008.
[25] T. Welton, Chemical reviews, 99 (1999) 2071-2084.
[26] P. Wasserscheid, W. Keim, Angewandte Chemie International Edition, 39 (2000) 3772-3789.
[27] B.C. Ranu, A. Das, S. Samanta, Journal of the Chemical Society, Perkin Transactions 1, (2002) 1520-1522.
[28] V. Calo, A. Nacci, L. Lopez, N. Mannarini, Tetrahedron Letters, 41 (2000) 8973-8976.
[29] T. Osako, A. Ohtaka, Y. Uozumi, Catalyst Immobilization, (2019) 325-368.
[30] V.V. Ramesh, S.S. Kale, A.S. Kotmale, R.L. Gawade, V.G. Puranik, P. Rajamohanan, G.J. Sanjayan, Organic letters, 15 (2013) 1504-1507.

[31] J. Zhang, Q. Liu, C. Duan, Y. Shao, J. Ding, Z. Miao, X.-Z. You, Z. Guo, Journal of the Chemical Society, Dalton Transactions, (2002) 591-597.
[32] M. Lamac, J. Tauchman, I. Císařová, P. Štěpnička, Organometallics, 26 (2007) 5042-5049.
[33] M. Ito, T. Ootsuka, R. Watari, A. Shiibashi, A. Himizu, T. Ikariya, Journal of the American Chemical Society, 133 (2011) 4240-4242.
[34] H.A. Zamani, G. Rajabzadeh, M. Masrornia, A. Dejbord, M.R. Ganjali, N. Seifi, Desalination, 249 (2009) 560-565.
[35] M. Amirnasr, R.S. Erami, S. Meghdadi, Sensors and Actuators B: Chemical, 233 (2016) 355-360.
[36] S. Meghdadi, M. Amirnasr, A. Amiri, Z.M. Mobarakeh, Z. Azarkamanzad, Comptes Rendus Chimie, 17 (2014) 477-483.
[37] J. Sumner, K. Weber, L. Hockett, S. Creager, The Journal of Physical Chemistry B, 104 (2000) 7449-7454.
[38] M. Shionoya, K. Tanaka, Current Opinion in Chemical Biology, 8 (2004) 592-597.
[39] M.V. de Souza, C.F. da Costa, V. Facchinetti, C.R.B. Gomes, P.M. Pacheco, Current Organic Synthesis, 16 (2019) 244-257.
[40] K. Ishihara, T. Yano, Organic letters, 6 (2004) 1983-1986.
[41] E. Bald, K. Saigo, T. Mukaiyama, Chemistry Letters, 4 (1975) 1163-1166.
[42] A. Amiri, M. Amirnasr, S. Meghdadi, K. Mereiter, V. Ghodsi, A. Gholami, Inorganica Chimica Acta, 362 (2009) 3934-3940.
[43] S. Meghdadi, M. Amirnasr, M. Zhiani, F. Jallili, M. Jari, M. Kiani, Electrocatalysis, 8 (2017) 122-131.
[44] M.P. Doyle, B.D. Brandes, A.P. Kazala, R.J. Pieters, M.B. Jarstfer, L.M. Watkins, C.T. Eagle, Tetrahedron letters, 31 (1990) 6613-6616.
[45] K. Si Larbi, H.Y. Fu, N. Laidaoui, K. Beydoun, A. Miloudi, D. El Abed, S. Djabbar, H. Doucet, ChemCatChem, 4 (2012) 815-823.
[46] G. Molteni, C.L. Bianchi, G. Marinoni, N. Santo, A. Ponti, New J. Chem., 30 (2006) 1137-1139.
[47] L. Liang, D. Astruc, Coord. Chem. Rev., 255 (2011) 2933-2945.
[48] M.A. Tasdelen, Y. Yagci, Tetrahedron Lett., 51 (2010) 6945-6947.
[49] S. Roy, T. Chatterjee, M. Pramanik, A.S. Roy, A. Bhaumik, S.M. Islam, J. Mol. Catal. A: Chem., 386 (2014) 78-85.
[50] A. Azam, A.S. Ahmed, M. Oves, M. Khan, A. Memic, International journal of nanomedicine, 7 (2012) 3527.
[51] X-Area WinXpose 2.0.22.0 (STOE, Darmstadt, Germany.
[52] X-Area Recipe 1.33.0.0 (STOE, Darmstadt, Germany.
[53] X-Area X-Red32 1.63.2.0 (STOE, Darmstadt, Germany.
[54] X-Area Integrate 1.71.0.0 (STOE, Darmstadt, Germany.
[55] G.M. Sheldrick, Acta Crystallographica Section A: Foundations and Advances, 71 (2015) 3-8.
[56] G.M. Sheldrick, Acta Crystallographica Section C: Structural Chemistry, 71 (2015) 3-8.
[57] C.E. Elwell, B.D. Neisen, W.B. Tolman, Inorganica chimica acta, 485 (2019) 131-139.
[58] E. Aktan, A.B. Gündüzalp, Ü.Ö. Özmen, Journal of Molecular Structure, 1128 (2017) 775-784.
[59] S.H. Sumrra, M. Hanif, Z.H. Chohan, M.S. Akram, J. Akhtar, S.M. Al-Shehri, Journal of enzyme inhibition and medicinal chemistry, 31 (2016) 590-598.
[60] I. Lumb, B.S. Sran, H. Sood, D.S. Arora, G. Hundal, Polyhedron, 127 (2017) 153-166.
[61] S.M. Pourmortazavi, M. Rahimi-Nasrabadi, F. Ahmadi, M.R. Ganjali, Journal of Materials Science: Materials in Electronics, 29 (2018) 9442-9451.
[62] M. Safaei, M. Taran, M.M. Imani, Materials Science and Engineering: C, 101 (2019) 323-329.
[63] S.S. Hussain, S. Al-Nuzal, S.F. Al-Qazzaz, J. Gen. Environ. Res. Conserv, 3 (2015) 173-187.
[64] R. Jenkins, R.L. Snyder, Introduction to X-ray powder diffractometry, 1996.
[65] V. Baco-Carles, L. Datas, P. Tailhades, ISRN Nanotechnology, 2011 (2011).

[66] S. Meghdadi, M. Amirnasr, M.H. Habibi, A. Amiri, V. Ghodsi, A. Rohani, R.W. Harrington, W. Clegg, Polyhedron, 27 (2008) 2771-2778.
[67] M. Amini, R. Hassandoost, M. Bagherzadeh, S. Gautam, K.H. Chae, Catalysis Communications, 85 (2016) 13-16.
[68] I. Jlalia, F. Gallier, N. Brodie-Linder, J. Uziel, J. Augé, N. Lubin-Germain, Journal of Molecular Catalysis A: Chemical, 393 (2014) 56-61.
[69] M. Bagherzadeh, H. Mahmoudi, S. Ataie, M. Hafezi-Kahnamouei, S. Shahrokhian, G. Bellachioma, L. Vaccaro, Inorganica Chimica Acta, 492 (2019) 213-220.
[70] W.S. Brotherton, (2012).
[71] W.G. Lewis, F.G. Magallon, V.V. Fokin, M. Finn, Journal of the American Chemical Society, 126 (2004) 9152-9153.
[72] J.E. Hein, V.V. Fokin, Chemical Society Reviews, 39 (2010) 1302-1315.
[73] K.R. Reddy, K. Rajgopal, M.L. Kantam, Synlett, 2006 (2006) 957-959.
[74] E. Haldon, M.C. Nicasio, P.J. Perez, Organic & biomolecular chemistry, 13 (2015) 9528-9550.
[75] Y. Jiang, D. Kong, J. Zhao, W. Zhang, W. Xu, W. Li, G. Xu, Tetrahedron letters, 55 (2014) 2410-2414.
[76] B. Roopashree, V. Gayathri, H. Mukund, Journal of Coordination Chemistry, 65 (2012) 1354-1370.
[77] S. Meghdadi, M. Amirnasr, M. Kiani, F. Fadaei Tirani, M. Bagheri, K.J. Schenk, Journal of Coordination Chemistry, 70 (2017) 2409-2424.
[78] M. Nasrollahzadeh, S.M. Sajadi, Journal of colloid and interface science, 457 (2015) 141-147.
[79] F. Nador, M.A. Volpe, F. Alonso, A. Feldhoff, A. Kirschning, G. Radivoy, Applied Catalysis A: General, 455 (2013) 39-45.
[80] N.A. Dangroo, A.A. Dar, B.A. Dar, Tetrahedron letters, 55 (2014) 6729-6733.
[81] M. Bagherzadeh, A. Bayrami, R. Kia, M. Amini, L.J.K. Cook, P.R. Raithby, Inorganica Chimica Acta, 466 (2017) 398-404.
[82] T.V. Tran, G. Couture, L.H. Do, Dalton Transactions, (2019).
[83] A.G. Mahmoud, M.F.C.G. da Silva, K.T. Mahmudov, A.J. Pombeiro, Dalton Transactions, 48 (2019) 1774-1785.
[84] K. Gonzalez-Silva, D. Rendon-Nava, A. Alvarez-Hernández, D. Mendoza-Espinosa, New Journal of Chemistry, 43 (2019) 16538-16545.

Table 1. Crystal data and structure refinement for $[Cu(L)_2(H_2O)].CH_3Cl$

Formula	$C_{19}H_{15}Cl_3CuN_6O_3S_2$
$D_{calc.}$/ g cm^{-3}	1.687
μ/mm^{-1}	1.454
Formula Weight	609.38
Colour	green
Shape	prism
Size/mm^3	0.35×0.10×0.04
T/K	292(1)
Crystal System	monoclinic
Space Group	$P2_1/n$
a/Å	9.8921(6)
b/Å	14.3386(6)
c/Å	16.9234(11)
α/°	90
β/°	92.123(5)
γ/°	90
V/Å^3	2398.7(2)
Z	4
Z'	1
Wavelength/Å	0.71073
Radiation type	Mo K□
Θ_{min}/°	1.862
Θ_{max}/°	29.223
Measured Refl's.	22878
Ind't Refl's	6476
Refl's with I > 2(I)	3492
R_{int}	0.0559
Parameters	341
Restraints	49
Largest Peak/e Å^{-3}	0.304
Deepest Hole/e Å^{-3}	-0.478
GooF	0.898
wR_2 (all data)	0.1026
wR_2	0.0842
R_1 (all data)	0.0968
R_1	0.0418

Table 2. Selected bond distances (°A) and angles (°) for $[Cu(L)_2(H_2O)].CHCl_3$ (**1**)

Bond lengths	
$Cu\text{-}N_5$	1.990(2)
$Cu\text{-}N_2$	2.006(2)
$Cu\text{-}N_6$	2.227(3)
$Cu\text{-}N_3$	2.027(3)
Bond angles	
$N_5\text{-}Cu\text{-}O_3$	89.17(10)
$N_5\text{-}Cu\text{-}N_2$	174.21(11)
$O_3\text{-}Cu\text{-}N_2$	93.18(10)
$N_5\text{-}Cu\text{-}N_3$	94.47(11)
$O_3\text{-}Cu\text{-}N_3$	158.68(11)
$N_2\text{-}Cu\text{-}N_3$	81.45(11)
$N_5\text{-}Cu\text{-}N_6$	77.67(10)
$O_3\text{-}Cu\text{-}N_6$	101.62(11)
$N_2\text{-}Cu\text{-}N_6$	106.98(10)
$N_3\text{-}Cu\text{-}N_6$	99.68(11)

Table 3. Hydrogen Bond information for $[Cu(L)_2(H_2O)].CHCL_3$ (**1**)

D	**H**	**A**	**d(D-H)/Å**	**d(H-A)/Å**	**d(D-A)/Å**	**D-H-A/deg**
O3	H3A	O2[1]	0.80(3)	1.91(3)	2.712(3)	173(5)
O3	H3B	N1	0.80(3)	1.87(3)	2.625(4)	158(5)

[1]-x,2-y,1

Table 4. The effect of time, temperature and the amount of catalyst on the cycloaddition of benzyl chloride with phenyl acetylene in the presence of sodium azide.[a]

Entry	Cat (mol %)	Temp (°C)	Time (h)	Yeild (%)[b]
1	-	70	12	0
2	**1**(0.54)	70	6	79
3	**1**(1.03)	70	6	81
4	**1**(1.55)	70	6	88
5	**1**(2.08)	70	6	92
6	**1**(2.59)	70	6	99
7	**1**(5.18)	70	6	99
8	**2**(0.27)	70	6	31
9	**2**(0.54)	70	6	58
10	**2**(0.81)	70	6	65
11	**2**(1.08)	70	6	80
12	**2**(1.35)	70	6	95
13	**2**(1.62)	70	6	95
14	**1**(2.59)	r.t.	6	11
15	**1**(2.59)	60	6	84
16	**1**(2.59)	50	6	78
17	**1**(2.59)	40	6	66
18	**2**(1.35)	r.t.	6	9
19	**2**(1.35)	60	6	79
20	**2** (1.35)	50	6	64

21	**2**(1.35)	40	6	44
22	**1**(2.59)	70	4	81
23	**2**(1.35)	70	4	57
24[c]	**1**(2.59)	70	6	99
25[c]	**2**(1.35)	70	6	93

[a]Reaction conditions: 0.5 mmol of phenylacetylene, 0.55 mmol of benzyl chloride, 0.55 mmol of sodium azide, 2 mL of H_2O.
[b] Isolated yields.
[c] The reactions were performed by adding sodium ascorbate as a reductant with a molar ratio of 2:1 of sodium ascorbate to the catalyst.

Table 5. Cycloaddition of alkyl halides with terminal alkynes in the presence of **1** and **2** and NaN_3 under the optimized reaction conditions.[a]

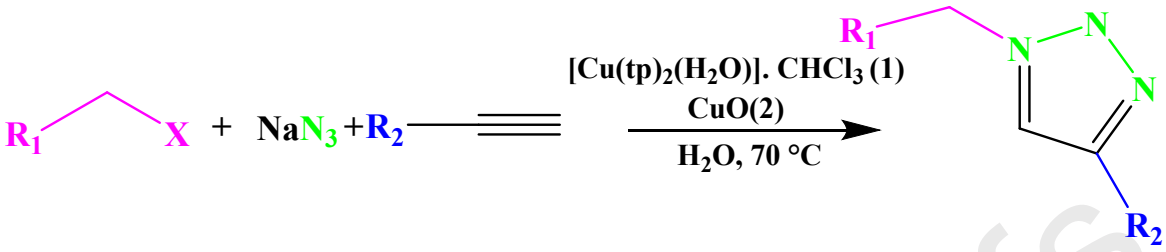

Entry	R_1	R_2	X	Yield (%)[b] Cu(II) complex(1)	Yield (%)[b] CuO(2)
1	Ph	Ph	Cl	99	95
2	4-Me-Ph	Ph	Cl	95	89
3	2-Me-Ph	Ph	Cl	91	80
4	4-NO_2-Ph	Ph	Cl	85	75
5	Ph	4-MeO-Ph	Cl	92	86
6	Ph	4-Me-Ph	Cl	90	83
7	Ph	CH_2OH	Cl	63	57
8	Ph	$(CH_3)_2COH$	Cl	59	48
9	Ph	Ph	Br	88	76
10	Ph	4-MeO-Ph	Br	92	74
11	Ph	4-Me-Ph	Br	84	68
12	Ph	CH_2OH	Br	63	43
13	Ph	$(CH_3)_2COH$	Br	47	41

[a] Reaction conditions: 0.5 mmol of terminal alkyne, 0.55 mmol of alkyl halide, 0.55 mmol of sodium azide, 2 mL of H_2O, 70 °C and 6 h

[b] Isolated yields.

Table 6. Recently reported catalytic systems for AAC in the presence of CuO nanoparticle.

Entry	Catalyst	Conditions	Yield(%)	Ref
1	Cu NPs	Catalyst (10 mol %) / 5 ml EtOH /5 h / 25 °C	95	[78]
2	$Cu(OAc)_2 \cdot H_2O$	Catalyst (20 mol %) / 3 ml H_2O /20 h / r.t.	77	[73]
3	Cu NPs/silica coated maghemite	Catalyst (4.3 mol %)/2 ml H_2O/2 h/70 °C	83	[79]
4	CuSO4-sodium Ascorbate	CuSO4-sodium ascorbate (10 mol % each)/15 ml acetone: water (1:1)/8.5 h/80 °C	89	[80]
5	$[CuL_2]$	Catalyst (0.86 mol%)/2 ml H_2O/14 h/70 °C	76	[69]
6	$[CuL_2]$	Catalyst (1.40 mol%)/2 ml H_2O/12 h/70°C	95	[81]
7	Cu-complex	Catalyst (50 µM)/0.15 mmol sodium ascorbate/10 ml H_2O/24 h/37°C	99	[82]
8	Cu-complex	Catalyst (3 mol%)/NaN_3 /1.5 ml H_2O/MeCN (1:1) /15 min/125°C/MW irradiation (10 W)	80.3	[83]
9	Cu-complex	Catalyst (2.5 mol%)/NaN_3 /5 ml MeOH/30 min/60°C/MW irradiation (30 W)	98	[84]
10	Cu(II) complex(**1**)	Catalyst (2.59 mol%)/ NaN_3 /2 ml H_2O /6h/70 °C	99	Present work
11	CuO NPs(**2**)	Catalyst (1.35 mol%)/ NaN_3 /2 ml H_2O /6h/70 °C	95	Present work

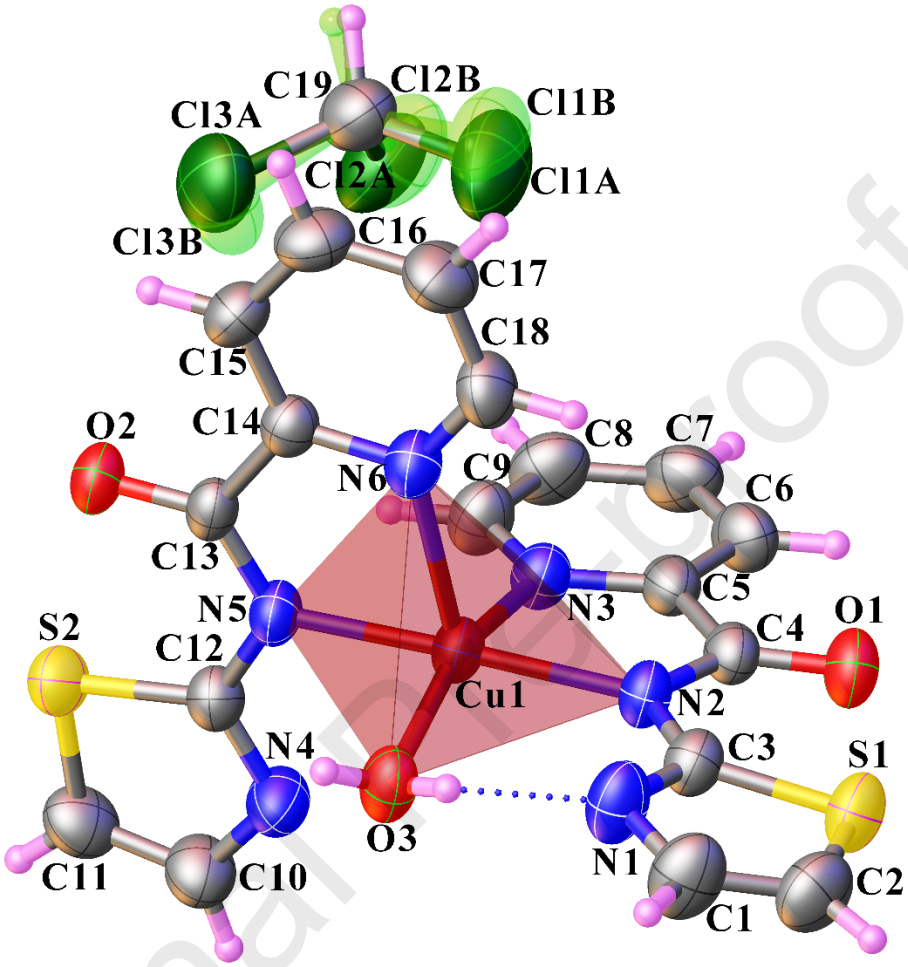

Fig. 1. The structure of $[Cu(L)_2(H_2O)].CH_3Cl$ (**1**) Displacements ellipsoids are drawn at the 50% level

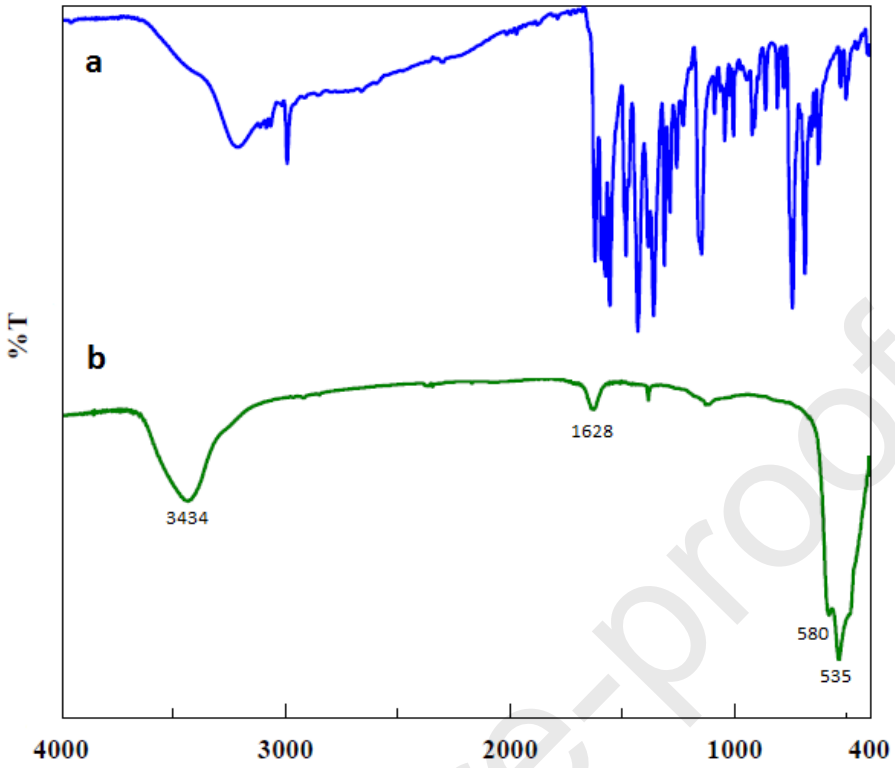

Fig. 2. FTIR spectrum of (a) $[Cu(L)_2(H_2O)].CHCL_3$ (b) CuO NPs

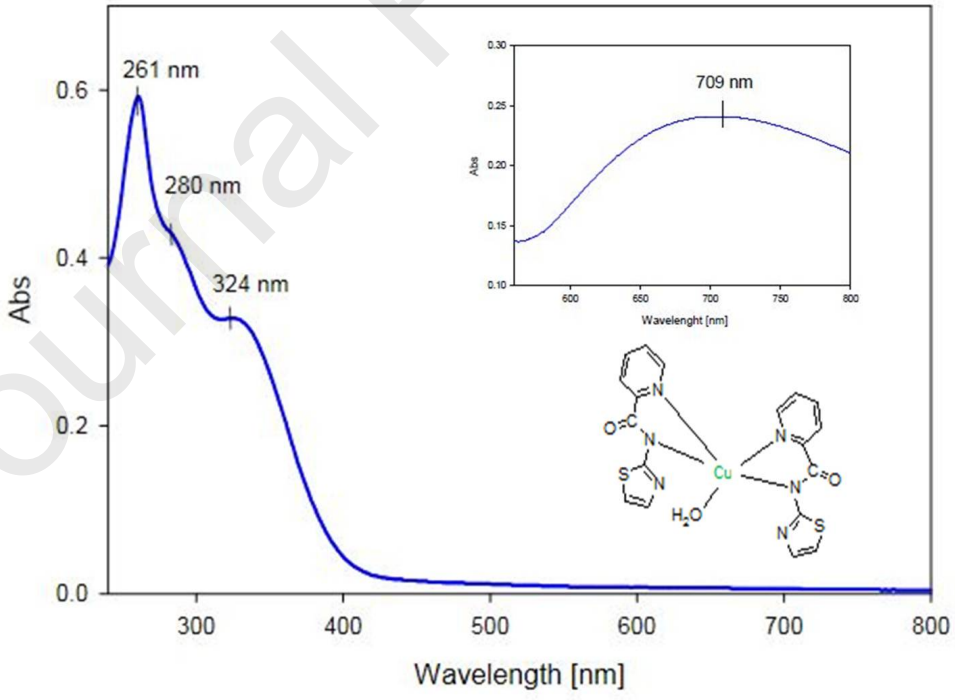

Fig. 3. Electron spectrum of the complex $[Cu(L)_2(H_2O)].CHCL_3$ (1.25×10^{-5} mol.lit^{-1} in acetonitrile solvent at 25°C)

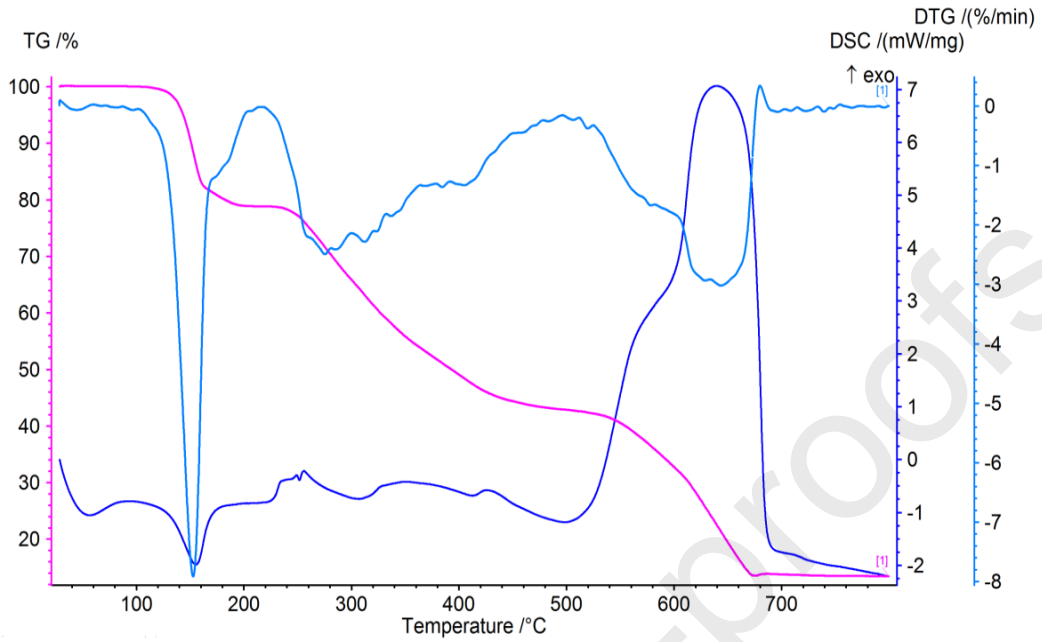

Fig. 4. TGA, DSG and DSC curves of [Cu $(L)_2(H_2O)$] $CHCl_3$ (**1**) complex precursor

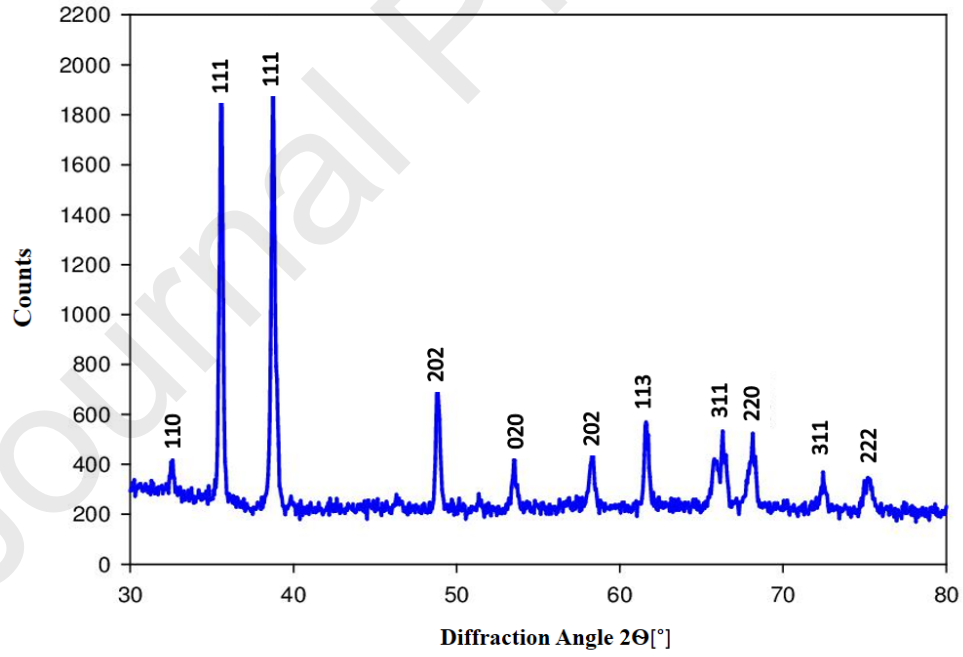

Fig. 5. X-ray (CuKα) powder diagram of the CuO NPs (**2**)

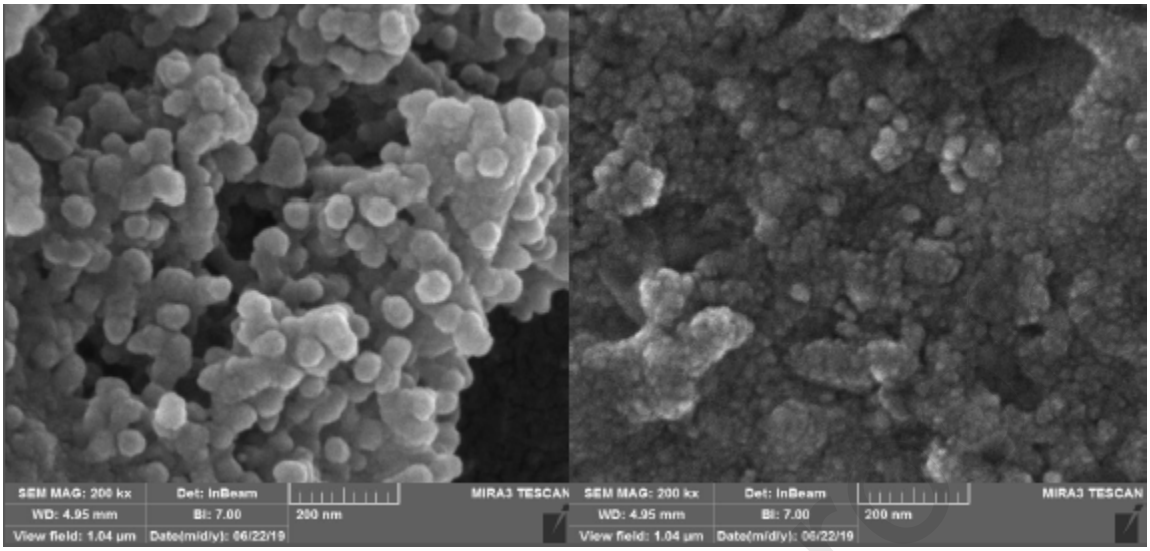

Fig. 6. FESEM images of the synthesized NPs of cupric oxide (**2**) (scale bar = 200nm)

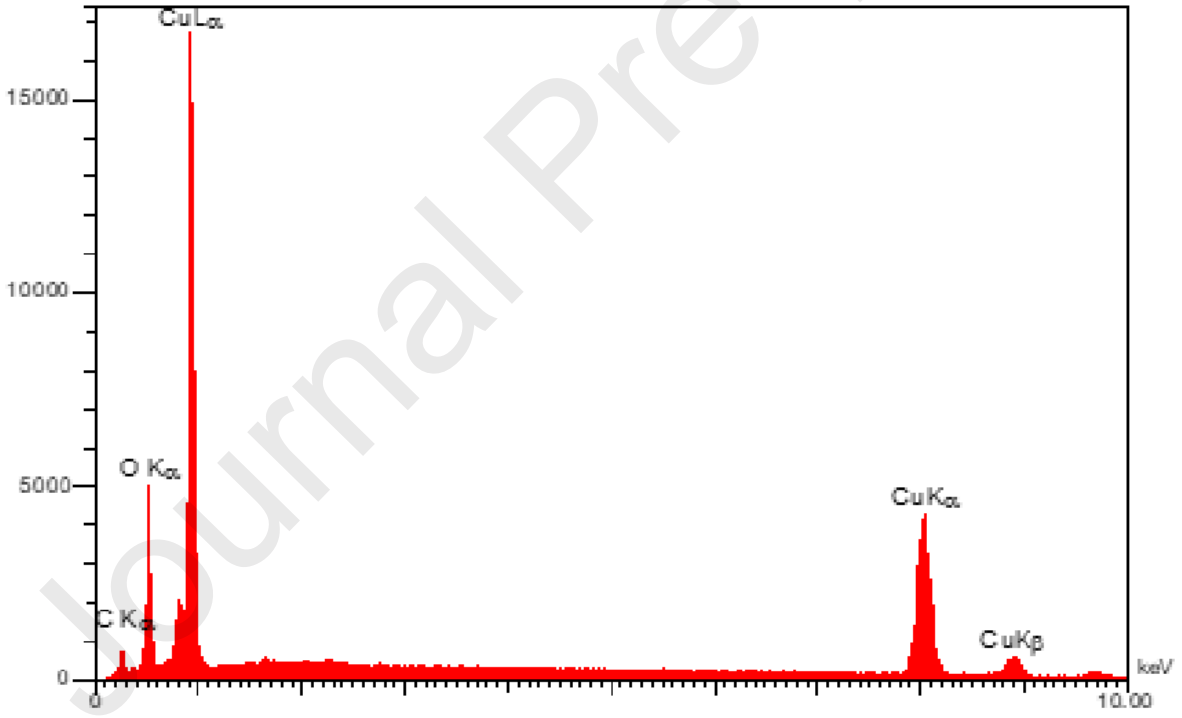

Fig 7. EDX spectrum of the CuO NPs (**2**)

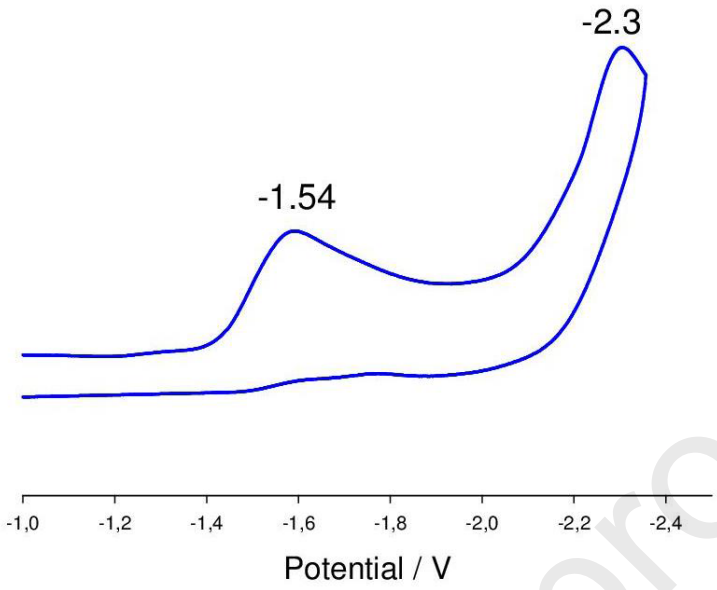

Fig. 8. Cyclic voltammogram of ligand in DMF at 298 K, c ≈ 5×10^{-3}, scan rate = 100 mV s^{-1}

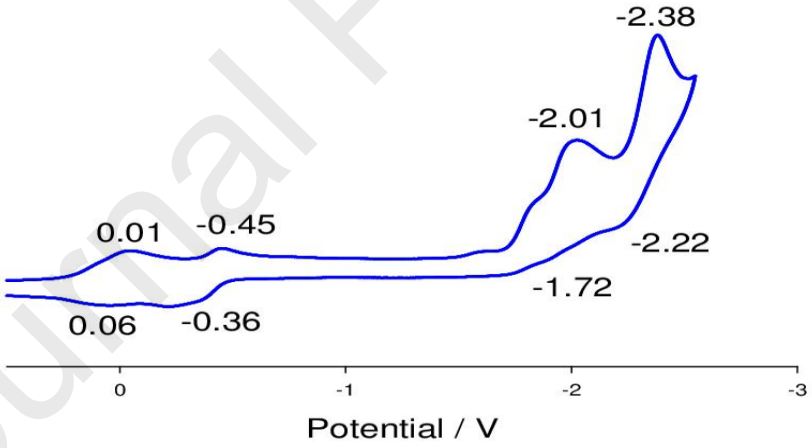

Fig. 9. Voltammogram of [Cu $(L)_2(H_2O)$] $CHCl_3$ Complex in DMF at 298 K, c ≈ 5×10^{-3}, scan rate = 100 mV s^{-1}

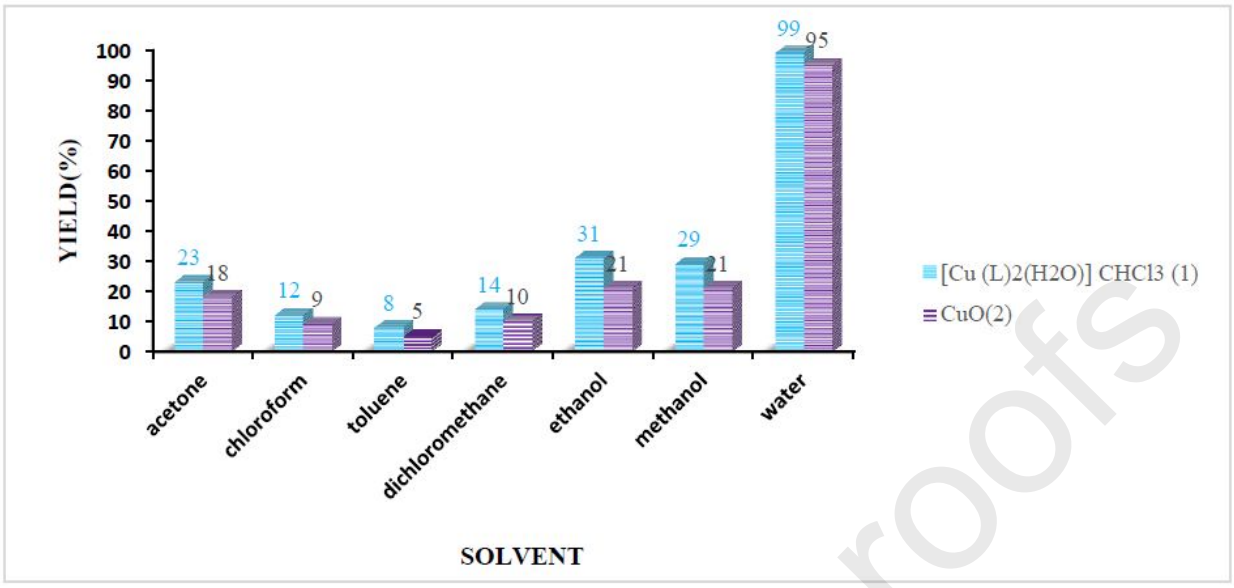

Fig. 10. Effect of solvent on the cycloaddition of benzyl chloride with phenyl acetylene and sodium azide.
[a]Reaction condition: 0.5 mmol of phenylacetylene, 0.55 mmol of benzyl chloride, 0.55 mmol of sodium azide, solvent 2 mL, 70°C, 6h
[b] Isolated yields.

Fig. 11. Reusability studies of the complexes **1** and **2** as a catalyst in the azide-alkyne cycloaddition reaction

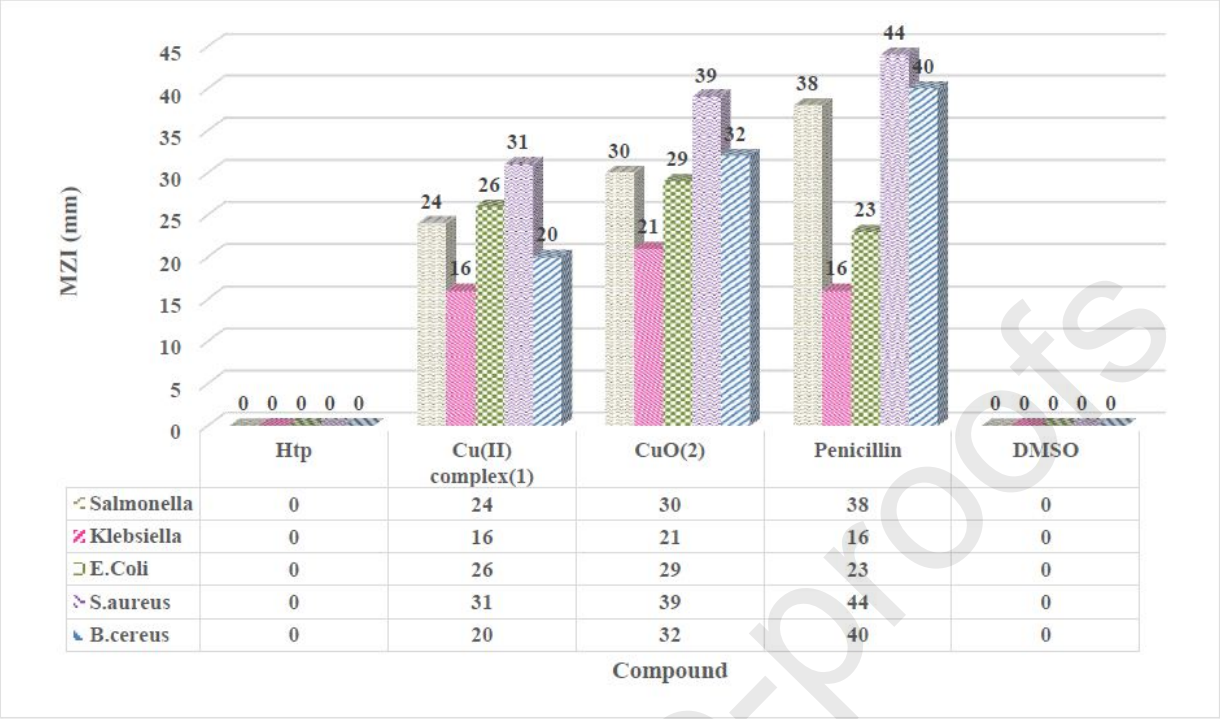

Fig. 12. MZI (mm) for the antibacterial activity of Htp, $[Cu(L)_2(H_2O)]$. $CHCl_3$ (**1**) and CuO(**2**)